

Spontaneous snap-through of strongly buckled liquid crystalline networks

Duygu Sezen Polat ^{a,b}, Michał Zmyślony ^c, John S. Biggins ^c, Danqing Liu ^{a,b,*}

^a Department of Chemical Engineering and Chemistry, Eindhoven University of Technology, Het Kraneveld 14, Eindhoven, 5600 MB, Netherlands

^b Institute for Complex Molecular Systems, Eindhoven University of Technology, Het Kraneveld 14, Eindhoven, 5600 MB, Netherlands

^c Department of Engineering, University of Cambridge, Trumpington St, Cambridge, CB2 1PZ, United Kingdom

ARTICLE INFO

Keywords:

Bistability
Snap-through
Rapid actuation
Liquid crystalline network
Responsive materials

ABSTRACT

The field of soft robotics is ever-changing, and substantial effort is allocated towards designing highly versatile and adaptable machines. However, while the soft robots demonstrate exceptional delicacy and flexibility, their ability to release energy in short timescales is rather unremarkable in contrast to their rigid predecessors. One of the routes to remedy that is to utilise mechanical instabilities, which are capable of accumulating substantial amounts of elastic energy and then releasing it in a very short period of time. In this work, we demonstrate a novel design of partially active liquid crystal network strips, which are then mechanically buckled and then snap-through due to the change in temperature. The experimental work combined with the numerical simulations demonstrate remarkable agreement and show different instability modes of various strengths. We provide a fundamental understanding of what governs the modes and how they can be accessed. The strongest mode results in snap-throughs taking as little as 6 ms with peak speeds as high as 60 cm/s for systems only a few millimetres in size.

Soft materials allow operations that are not possible with rigid actuators. They are highly versatile and adaptable to dynamic environments. However, they are also often slow, and limited to modest forces [1]. Nature can be a source of inspiration to overcome the intrinsic limitations of soft robots. For example, upon sensing the existence of a prey, a Venus flytrap can close its leaves in as little as 100 ms. The plant achieves this remarkable speed by employing an elastic snap-through instability. Generically, such an instability occurs when an equilibrium state for a system either ceases to exist or becomes unstable, as a control parameter changes and the system has to ‘jump’ to another stable state [2].

Previously, snappers have been engineered using a range of actuating soft materials stimulated by swelling [3–6], magnetic fields [7] and electric current [8]. In this work, we focused on polymer networks with liquid crystal (LC) alignment. Such LC solids actuate on heating by contracting along the alignment and expanding laterally, and can be prepared on a spectrum from stiff low-strain glasses to soft high-strain elastomers [9,10]. A key advantage of such LC materials is that they can be fabricated with spatial patterns of alignment direction, which deliver corresponding patterns of contraction on heating, leading to sophisticated programmed morphing [10–15]. Such programmed actuation allows a single monolithic LC actuator to behave as a sophisticated machine [16], achieving functions such as lifting [17], gripping [18], swimming [19,20], walking [21,22] and pumping [23,24].

Several different snapping LC actuators have been studied previously. The common theme is that a thickness gradient of actuation induces a spontaneous bending curvature, as familiar from bi-metal strips [25]. For snapping to result, this bending actuation must compete with another antagonistic source of curvature such as pre-buckling of a flat strip [26], or fabrication in the form of a curved shell [27,28] or other pre-curved geometry [29,30]. In some very elegant cases, LC morphing creates the two antagonistic curvatures sequentially, leading to specimens that start flat, actuate into one curved form then snap to another [31,32]. However, a ubiquitous feature of all these approaches is that the bending actuation is achieved with a thickness gradient of stimulation [26,27,29–31], lamination of two materials [28] or both [32].

In this work, we design a monolithic LC actuator that snaps even under uniform stimulation, due to its programmed contraction. Precisely, we present a liquid crystalline network (LCN) strip, fabricated with an active, splay-bend aligned part in the centre and a passive, isotropic part near the edges. The strip is buckled between two clamps making a bistable arch. Heating then generates preferred curvature in the central portion that snaps the arch to the opposite state. Because the actuation pattern is directly programmed into the LCN during fabrication, the result snaps very robustly, in quasistatic or dynamic/noisy stimulation. The material-programmed design is also scale-free, making it much

* Corresponding author at: Department of Chemical Engineering and Chemistry, Eindhoven University of Technology, Het Kraneveld 14, Eindhoven, 5600 MB, Netherlands.

E-mail addresses: jsb56@cam.ac.uk (J.S. Biggins), D.Liu1@tue.nl (D. Liu).

<https://doi.org/10.1016/j.eml.2024.102149>

Received 7 December 2023; Received in revised form 2 February 2024; Accepted 6 March 2024

Available online 11 March 2024

2352-4316/© 2024 The Author(s). Published by Elsevier Ltd. This is an open access article under the CC BY license (<http://creativecommons.org/licenses/by/4.0/>).

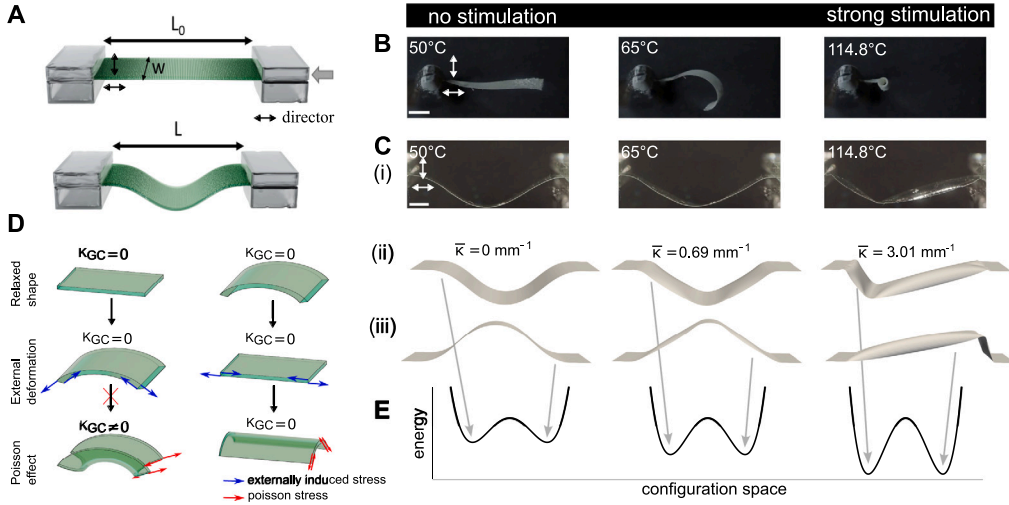


Fig. 1. Schematic and behaviour of fully splay-aligned LCN strip. **A** System schematic with four relevant dimensions in the experiment, thickness t , strip's length L_0 , clamping distance L and width w . **B** Splay aligned LCN strip clamped on one side curls in response to increased temperature. **C** Fully splay-aligned LCNs strips do not snap from the bottom to the top configuration both experimentally (i) and in simulations starting in the bottom configuration (ii) and the top (iii). **D** The transverse curvature is the result of the Poisson effect, which causes the curved sheets to curve transversely when longitudinally straightened. **E** Schematics of the energy landscape for the strip before and after being stimulated intermediately and strongly. In all three cases, the strip is bi-stable with an energy barrier in between preventing the snap-through from occurring.

easier to miniaturise than approaches relying on absorption length-scales, temperature gradients or other forms of patterned stimulation. Interestingly, despite the splay-bend alignment providing only bending deformation along the length of the strip, we also observe the formation of spontaneous curvature in the width direction on heating. This additional curvature provides a second type of antagonistic curvature to reinforce the pre-snapped state, delaying the instability and ultimately magnifying the released energy. Consequently, we observe exceptionally high power densities for a system made of such a soft material. We provide a straightforward explanation of this phenomenon which is supported by both experimental demonstrations and numerical simulations.

1. Results and discussion

1.1. Fully active strips

We fabricated LCNs by photo co-polymerisation of LC monomers at nematic temperature (Fig. S1). Initially, we worked with LCNs that possess a splay-bend alignment along the whole length, where the molecules transition from a planar orientation to a perpendicular orientation across the thickness of the film. When the order parameter is reduced, the planar side of the LCN contracts while the homeotropic (perpendicularly aligned) side expands, causing the film to initiate bending (curling) towards the planar side as shown in Figs. 1B and S2 [11,33]. The strip is initially pre-buckled, which makes the strip's energy landscape have two minima — downwards and upwards buckling configurations, whereas the preferred curvature is meant to shift the energy landscape, such that downwards state becomes unstable. The idea is to pre-buckle the strip downwards, giving its centre positive curvature, and then induce negative preferred curvature through heating to cause the strip to snap upwards.

Typically, a splay film of the length $L_0 = 16$ mm, width $w = 4$ mm and thickness $t = 20$ μ m is used. This strip was clamped flatly at its ends and buckled by moving the clamps closer together to a shorter distance L as shown in Fig. 1A. We will use a short-hand notation for the strip's dimensions $L_0/L/w$ with dimensions in millimetres. Throughout all experiments and simulations, the samples are initially set with a planar alignment at the bottom and a homeotropic alignment at the top.

In the first experiment, a splay-aligned strip with dimension 16/14/4 was placed inside an oven at a temperature of 20 °C. The strip

was then heated at a gradual rate of 5 °C per minute until it reached a temperature of 115 °C. Interestingly, no snapping was observed, with the strip morphing but remaining in the downward configuration. Matching numerical simulations (Morphoshell [34]) showed good agreement on shape evolution on stimulation, and confirm the lack of snapping (Fig. 1C). In hindsight, the lack of snapping stems from the presence of both signs of curvature in the downward pre-buckled strip: positive in the middle and negative near the clamps. Indeed, if the left and right halves of the downward configuration are switched one obtains the upward configuration, revealing that, on symmetry grounds, the two states have the same energy. Actuation thus reinforces the bi-stable energy landscape, and does not destabilise the downward configuration (Fig. 1E).

However, the experiments and simulations do show a surprising behaviour on stimulation: both strips develop long regions that are longitudinally (\parallel) straight, but curved in the transverse width direction (\perp), despite the fact that splay-bend produces purely longitudinal preferred curvature [33]. To rationalise this behaviour, we recall the bending energy surface density of a spontaneously curved ribbon

$$W = \frac{D}{2} \left((1 - \nu) \text{Tr}((\kappa - \bar{\kappa})^2) + \nu (\text{Tr}(\kappa - \bar{\kappa}))^2 \right), \quad (1)$$

where D is the bending stiffness, ν the Poisson ratio, $\kappa = \text{diag}(\kappa_{\parallel}, \kappa_{\perp})$ is the obtained curvature tensor and $\bar{\kappa} = \text{diag}(\bar{\kappa}, 0)$ is the preferred curvature tensor induced by splay-bend. From this energy, we see that the experimental transverse curvature arises as a Poisson effect. For a given longitudinal curvature, the energy is minimised by the transverse curvature

$$\kappa_{\perp} = -\nu(\kappa_{\parallel} - \bar{\kappa}), \quad (2)$$

so a transverse curvature is beneficial whenever there is a mismatch between the preferred and obtained longitudinal curvatures. Such Poisson bends are somewhat unfamiliar because they are not actually observed when bending flat sheets, even though they would indeed reduce the bending energy. Precisely, if a naturally flat sheet is bent longitudinally, this Poisson effect would cause it to curve anti-clastically in the perpendicular direction as shown in Fig. 1D. However, this would cause the strip to obtain non-zero Gauss curvature ($K_{GC} = \kappa_{\parallel}\kappa_{\perp}$), which as known from *theorema egregium* would cost stretching energy, which for thin sheets is substantially more costly than bending energy. Thus anti-clastic suppression is observed [35] and only the mechanically induced

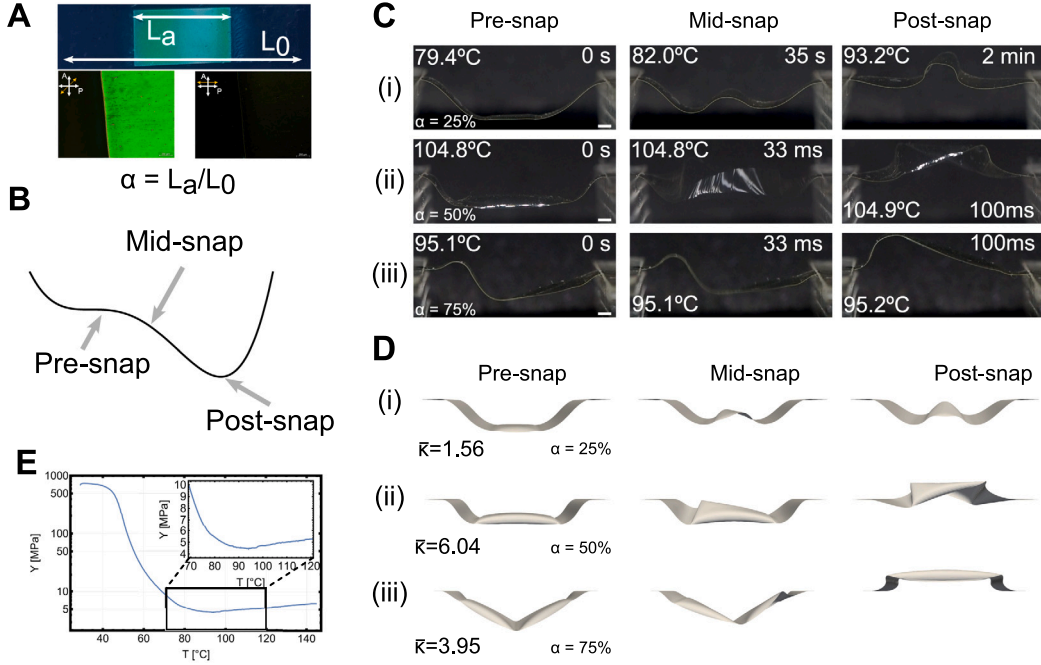


Fig. 2. Quasi-static snapping of partially active LCN strips. **A** Picture of the partially active LCN film between crossed polarisers. The birefringent part is splay-aligned and the isotropic one is polydomain. The ratio of lengths is the active ratio $\alpha = L_a/L_0$. **B** Schematics of the energy landscape at the threshold. The initial pre-snap shape becomes unstable and goes through a sequence of unstable configurations before reaching the only remaining equilibrium state. **C** Snapshots from experiments of the 16/14/4 strip for three different active ratios. The temperature corresponds to the temperature at which the given strip has snapped, and the timestamps are in reference to the last frame before the snapping has begun. **D** Simulated snap-through pathways of strips with three different active ratios, with marked threshold curvature. The active segments are offset by 1% of the length. Fig. S2 shows the dependence of curvature from temperature for comparison. **E** Storage modulus of polydomain LCN strip obtained by dynamic mechanical analysis.

curvature remains. However, if a strip with natural longitudinal curvature is mechanically straightened out, it prefers to bend transversely

$$\kappa_{\perp} = \nu \bar{\kappa}, \quad (3)$$

and can attain this curvature without stretch, as the strip is now longitudinally straight. In our system, the clamps impose the constraint that $\int \kappa_{\parallel} ds = 0$, preventing the strip from developing additional longitudinal curvature in response to increasing $\bar{\kappa}$. Ultimately this motivates a longitudinal phase-separation, where most of the strip becomes longitudinally straight, allowing it to attain a Poisson transverse curvature $\nu \bar{\kappa}$, and thereby save an energy $W \sim D\nu^2 \bar{\kappa}^2$.

Furthermore, this transverse curvature does not interfere with the symmetry argument relating up and down states, as the upward configuration can still be formed by a piece-wise rearrangement of the downwards configuration. This symmetry argument neglects a small difference between the central and clamped “hinges” in the structure, but simulations reveal that these induce an energy difference of no more than a few percent, with the barrier between the two states deepening with actuation, rather than disappearing.

For the snap-through to occur the system needs to favour one of the configurations, while a uniform stimulation of splay aligned strip only reinforces the original bi-stable system as shown in Fig. 1E. One method of biasing is to use local stimulation, such as illumination of the centre part as was done by Shankar et al. [26]. However, we propose an alternative design by encoding the bias directly into the strip’s design by establishing the splay alignment exclusively in the central part while maintaining the remaining sections of the film in a passive isotropic state.

1.2. Active and passive segments

In order to do that, we polymerised the central part of the strip in the nematic state to lock in the splay alignment while covering the rest of the strip with a photomask. Once the central part was cured, the

sample was heated to the isotropic state, where the rest of the strip was polymerised. This resulted in a strip containing an active splay-aligned segment in the centre and the passive polydomain segment, correspondingly seen as birefringent and non-birefringent regions in Figs. 2A and S3. The role of the passive sections is two-fold: firstly, they eliminate the stresses at the clamps and secondly, they do not favour either configuration, while the central, active part now favours only the top one and the energy difference between the states will increase with stimulation. Once an active segment is introduced to the system the top-bottom symmetry is broken and while for weak stimulation it is still bi-stable with the energy landscape with two minima separated by an energy barrier, for stronger stimulation the energy barrier disappears (Fig. 2B) and instability is observed.

1.3. Instability modes

We first focused on strips with active ratios ($\alpha = L_a/L_0$) of 25%, 50% and 75% which snapped through in distinctly different pathways (Fig. 2C). Surprisingly, despite the 50% active strip being expected to experience the strongest bias between the configurations, while it exhibited the fastest snap-through, it also required the largest temperature for it to occur. Conversely, the 25% active strip snapped the slowest while simultaneously requiring the lowest temperature. Furthermore, the snap-through of the 25% active strip had a very small amplitude which did not move its centre of mass above the height of the clamps, while both the 50% and 75% active strips snap-through in order of milliseconds once a threshold temperature is exceeded.

Using Morphoshell we simulated the deformations of the strips in a quasi-static manner by slowly increasing the magnitude of the preferred curvature in the active segment with equilibration between each increment. As the stiffness of the material at the temperatures characteristic of the instabilities was low ($Y \approx 4.5$ MPa, Fig. 2E), we included the influence of both elastic effects and gravity and included a 1% length offset (160 μ m) in the placement of the strip in order

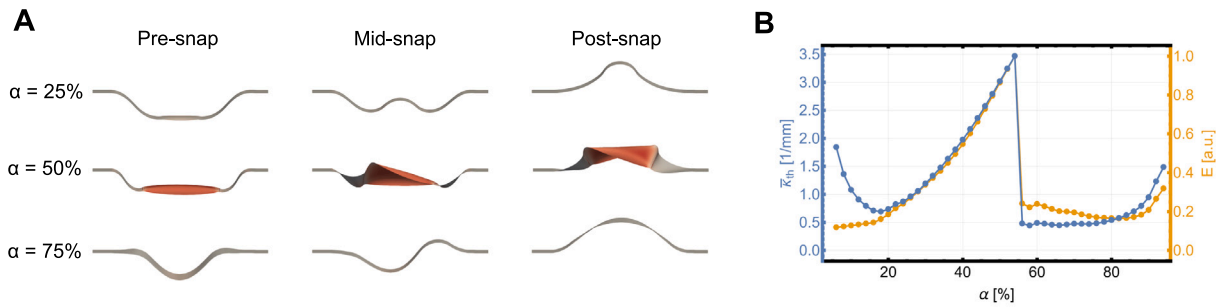


Fig. 3. Quasi-static snapping of partially active LCN strips in the absence of gravity. **A** Snap-through pathways of 25%, 50% and 75% active strip with red colour marking the bending energy density. **B** Theoretical snapping curvatures and released elastic energies for varying active ratio α for the 16/14/4 film. The Young modulus was taken to be 4.5 MPa. (For interpretation of the references to colour in this figure legend, the reader is referred to the web version of this article.)

to decrease the simulation's symmetry, as ideally symmetric placement is experimentally unattainable. This replicated the experimental behaviour to a very good degree (Fig. 2D).

In both the 25% and 50% active strips we first observe a loss of all longitudinal curvature in the active segment which is then replaced by transverse curvature before a snap-through occurs. The snap-through occurs along the diagonal of the active segment, where its two opposite corners rise while the other two initially remain immobile. This mode of snap-through requires the strip to partially lose its transverse curvature, therefore, the more transversely curved the strip is, the more delayed the snap-through will be.

As the variation of transverse curvature along the strip results in a Gauss curved shape, the rate at which the transverse curvature varies depends on the relative strength of stretching to bending. In the case of two strips that have the same dimensions but different active ratios, the one with more of an active segment will result in higher peak values of transverse curvature, delaying the snap-through, which explains why the 50% active strip requires significantly stronger stimulation than the 25% one.

However, the 75% active strip does not snap at a higher temperature but rather at a lower one than the 50% active strip. Upon investigation, we observe a difference in the snap-through mode, such as the strip does not lose all of its longitudinal curvature in the active segment but rather forms two transversely curved sections that are separated by a longitudinally curved part and one negatively longitudinally curved segment. As a result of this different configuration, the snap-through occurs via the growth of the longitudinally curved segment near the edge of the active segment, which drives the snap-through at an earlier stage than the previous mode.

To gain more insight, we then simplified the model by removing the influence of gravity from the simulations, which could correspond to a strip made of a stiffer material or a proportionally smaller system, and placing the strip fully symmetrically (Fig. 3). The behaviour of all the strips remains similar, however, all snap-throughs occur at lower thresholds of preferred curvature than with gravity. Without gravity, the 25% strip after the snap-through transitions fully to the upward configuration instead of remaining below the clamp height until the stimulus is significantly stronger. The snap-through of the 50% strips remains conceptually the same, first losing longitudinal curvature before snapping along the diagonal of the active segment. Interestingly, the strips with an active ratio greater than around 55% exhibit a drastically different snap-through pathway than those with a shorter active segment, where they retain regions of negative longitudinal curvature at the edges of the active segment, which allows them to transition at a vastly lower threshold (Fig. 3B). This indicates the existence of two separate snap-through modes which are dependent on the length of the active segment.

Therefore, we will distinguish three snap-through modes, unreinforced, partially reinforced and fully reinforced which can be accessed in order to control the properties of the snap-through. The unreinforced

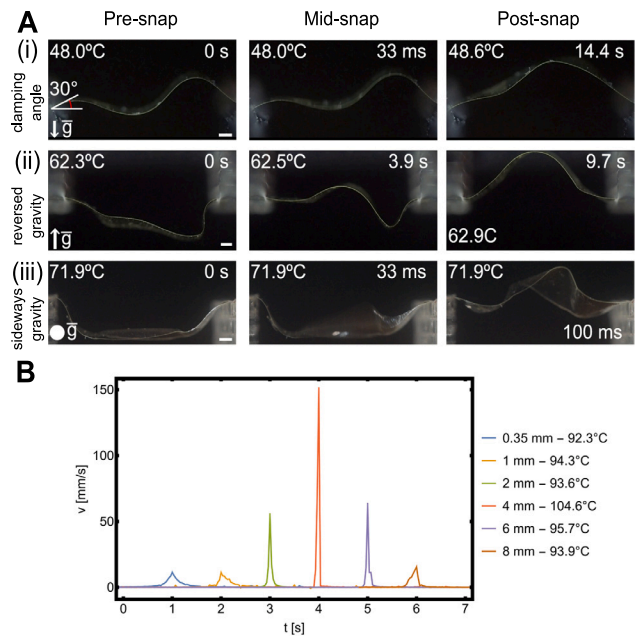


Fig. 4. Accessing different snap-through modes for the 16/14/4 50% active strip through system reconfiguration. **A** The same film as in A (i) snaps in the unreinforced mode if instead of having flat clamping, clamps are at an angle (here 30°). **(ii)** When gravity is helping the snap-through we see the unreinforced. **(iii)** When placed sideways in the oven we observe a reinforced mode. Scale bars correspond to 1 mm. **B** Velocity dynamics peaks corresponding to snap-through of strips with different widths placed on a common axis and offset for readability.

mode is the one where no significant amounts of transverse curvature develop and snap-through happens in a wave-like manner. In partially reinforced mode, the strip obtains significant amounts of transverse curvature, yet a negatively longitudinally curved segment exists, which lowers the threshold, in fully reinforced mode, no longitudinal curvature in the active segment remains and the strip snaps along the diagonal of the active segment.

1.4. Controlling the snap-through modes

Due to the presence of different modes, we investigated both experimentally and numerically whether it is possible to control the snap-through behaviour. When the gravity was acting against the snap-through, the strip exhibited fully reinforced instability and snapped at 104.8 °C (corresponding to $\bar{\kappa} = 5.78 \text{ mm}^{-1}$ in simulations for $Y = 4.5 \text{ MPa}$). However, if the 50% active strip is inverted upside-down, gravity promotes the snap-through, which occurs at a lower temperature of 62.3 °C (simulated $\bar{\kappa} = 0.11 \text{ mm}^{-1}$ for $Y = 18 \text{ MPa}$),

following the unreinforced instability as shown in Fig. 4A. When the strip is placed sideways in relation to gravity, it snaps at a temperature of 71.9 °C (simulated $\bar{\kappa} = 2.70 \text{ mm}^{-1}$ for $Y = 4.5 \text{ MPa}$) following the pathway of the fully reinforced instability. An alternative approach to modulating the modes is through mechanical biasing of the strip by setting the two ends at a positive angle, favouring the top configuration over the bottom one. This allows the snap-through to occur at a lower temperature of 48.0 °C (simulated $\bar{\kappa} = 0.25 \text{ mm}^{-1}$ for $Y = 100 \text{ MPa}$).

An alternative approach is to change the relative strength of stretching and bending energies by changing the geometry of the strip. The trade-off between the bending and stretching energies introduces a length scale $\mathcal{L} \sim \sqrt{Rl}$ which is the distance close to the edge of the strip where Gauss curvature can exist without a cost of stretching energy. Here, the R is the local radius of curvature, which will correspond with the characteristic radius of curvature due to buckling, and the relevant experimental length is w . Therefore, the dimensionless parameter Λ , defined as

$$\Lambda = \frac{w}{\mathcal{L}} = \sqrt{\frac{1 - L/L_0}{L_0 t}} w, \quad (4)$$

can be used to determine at which point the stretching becomes significant in the problem and when stretch reinforcement can occur. For sufficiently low values of Λ , the strip is expected to behave as if there was no constraint on the Gauss curvature and snap-through in the simple bend mode.

Similarly, if the strip becomes too wide, the effect of flat clamping of the strip's ends will propagate throughout the length of the strip inhibiting the development of transverse curvature. This is caused by the fact that the variation of transverse curvature along the length of the strip causes it to be Gauss' curved, and thus has a related stretching energy. The wider the strip is, the higher this energetic cost is, and both the rate of change and the final magnitude of transverse curvature are lower, with the limit of a strip of infinite width being a strip transversely flat. This indicates the existence of an optimal width, at which both the threshold curvature and the released energy per unit width, and, therefore, the speed, will be the greatest.

In order to test this theory, we fabricated strips with a 50% active ratio and dimensions $16/14/w$, where w ranged between 0.35 mm and 8 mm. As expected, the narrower strips exhibit snap-throughs at lower temperatures and release less energy, which is shown in Fig. 4B and likewise do the wider strips, with the $16/14/4$ strip having both the fastest snap-through and the highest threshold temperature.

The strong width dependence highlights the influence of transverse curvature, as in its absence, both the energy and the mass of the object would be linear in width, and thus, the dynamics would be width-independent.

1.5. Photothermal actuation

By subjecting the strip to uniform and gradual heating in the oven, we provide a consistent and slow increase in preferred curvature that allows the strip to transition through equilibrium states. This process revealed the presence of distinct modes of instability with varying strengths. However, for the snapping strip to be used as a force-generating mechanism, the requirement of having it enclosed in an oven is highly restrictive. Conversely, light-triggered stimulation offers a long-distance and untethered method of actuation. Therefore, we incorporated a near-infrared (NIR) photoabsorbent dye into the LCN and used NIR light for photothermal actuation (Fig. S4).

Firstly, we confirmed that 50% active ratio offers the fastest snap-through for the same actuation parameters, with peak speeds as high as 640 mm/s (Fig. 5A and B). In the case of photoactuation, the speed measurements are significantly more reliable, as a lower timeframe of the stimulation allows for recording with a high-speed camera. However, the photoactuation snap-through follows a different path than the oven actuation, with a less distinct modal structure, as shown

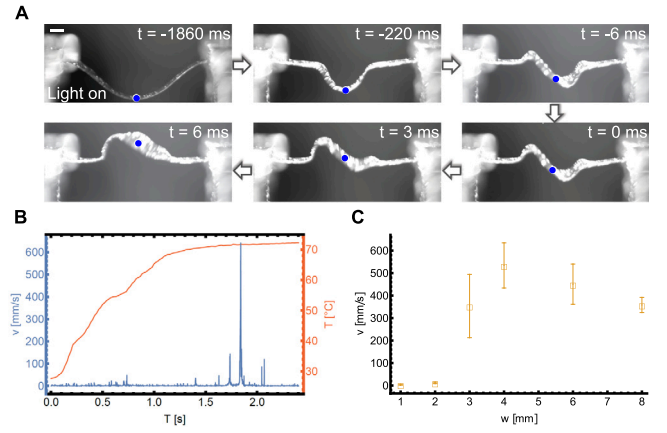


Fig. 5. Photothermal snap-through of LCN film. A High-speed camera snapshots of photothermal snap-through. The scale bar corresponds to 1 mm. B Kinetics of snap-through for 50% active 16/14/4 strip. C Exploration of stretch-reinforced snap-through.

in Fig. 5A and Mov. M6. This stems from the inhomogeneity of the light source, coupling between the strip's local angle and absorption, and the different heat conductivity in the centre of the strip and the ends, where due to the contact with clamps, the strip cools faster.

In order to check whether the stretch-bend competition still plays a significant role in the actuation, we compared the snap-through dynamics of strips with dimensions of $16/14/w$ where w ranged from 1 mm to 8 mm, and indeed there was a significant range of speeds with the narrowest strips snapping at peak speeds of 3.6 mm/s and the widest at 358.2 mm/s (Fig. 5C, dynamics in Fig. S5) with 4 mm wide strip being the fastest once again.

Similarly as before, the actuation can be modified by changing whether gravity is helping or acting against the snap-through, however, for photoactuation, the difference was less pronounced (Fig. S7). Most likely the reason behind that is the fact that the stiffness of the strips were closer to each other at the reached temperatures. Alternatively, one can change the buckling compression to increase the natural curvature of the strip. While it increases the released energy, it also increases the threshold curvature, which can inhibit the snap-through (Fig. S8).

1.6. Snap-through for object propulsion

Lastly, we demonstrate that our snapping strip can exert force by throwing an object, as shown in Fig. 6. To do so, we placed an object 50% heavier than the strip. In the oven, the bottom mode became even more stable than before and exhibited the snap-through transition at a higher temperature of 117.8 °C, which propelled the object 4.3 mm into the air (Fig. 6A). When the strip was actuated with light the object was propelled by 3.8 mm (Fig. 6B). These correspond to power densities of 35 kW/m³ and 44 kW/m³.

2. Conclusion

In this work, we designed an LCN system with instability encoded into its structure with splay and isotropic regions in the strip. We then demonstrated the presence of multiple modes of instability in this system created by the strong buckling of a splay-aligned strip. Due to the clamping, the strip cannot obtain its preferred shape and thus obtains a transversely curved shape, which for certain geometries prevents the low-energy-low-threshold bend mode from occurring and only after stronger actuation can it exhibit the snap-through instability. The instability mode behaviour is material-independent and can be used for different materials with other strain-temperature dependencies or stiffnesses. As the LCN used for the development of this system was relatively soft at its operating temperatures, the snapping behaviour

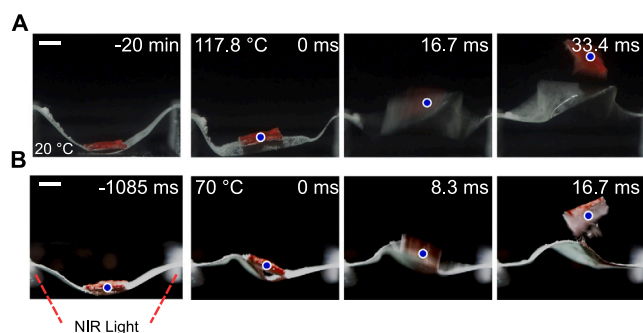


Fig. 6. Application of the spontaneous snap-through to perform throwing task A 16/14/4 50% strip placed into oven and heated with a rate of 5 °C/min. B 16/14/4 50% strip illuminated from the bottom with NIR light to initiate snap-through. Scale bars correspond to 2 mm.

was heavily influenced by gravity and just by changing the orientation of the sample, different thresholds and modes became accessible. If needed, by using a stiffer material, this influence can be minimised so that the snapping mode will be insensitive to configuration, and at the same time, the released energy will be increased. By controlling the geometry, different modes can be accessed in order to release large amounts of energy even when using a soft material. Snap-through design presented in this work may be used to develop strong actuators for soft robotics.

CRediT authorship contribution statement

Duygu Sezen Polat: Writing – review & editing, Writing – original draft, Visualization, Methodology, Investigation, Formal analysis. **Michał Zmysłony:** Writing – review & editing, Visualization, Software, Methodology, Formal analysis, Data curation. **John S. Biggins:** Writing – review & editing, Supervision, Funding acquisition, Conceptualization. **Danqing Liu:** Writing – review & editing, Supervision, Funding acquisition, Conceptualization.

Declaration of competing interest

The authors declare that they have no known competing financial interests or personal relationships that could have appeared to influence the work reported in this paper.

Data availability

Data will be made available on request.

Acknowledgements

We thank Charlotte Bording for drawing the schematic illustration of the LCN snapper and Dirk J. Broer for his comments on the manuscript. D.L. acknowledges financial support from the Netherlands Organisation for Scientific Research (OTP 19440, NWO OCENW.KLEIN. 10854, START-UP 8872 and NWO Sectorplan) and J.S.B. the support of UKRI ‘future leaders fellowship’ grant (grant no. MR/S017186/1). This work is funded by the European Union’s Horizon 2020 Research and Innovation Programme under the Marie Skłodowska-Curie Grant Agreement No. 956150 (STORM-BOTS).

Appendix A. Materials and methods

A.1. Materials

The reactive mesogens 1,4-di-[4-(6-acryloyloxyhexyloxy)benzoyloxy]-2-methylbenzene (1), 4-Methoxyphenyl 4-(6-(acryloyloxy)

hexyloxy)benzoate (2) and 4-Cyanophenyl 4-((6-(acryloyloxy)hexyl)oxy)benzoate (3) were obtained from Merck UK. Photoabsorbent dye Lumogen 788 (4) was received from BASF. Phenylbis(2,4,6-trimethylbenzoyl)phosphine oxide (5) was obtained from CIBA. Butylated hydroxytoluene (6) was purchased from Sigma Aldrich. Dichloromethane (DCM) was purchased from Sigma-Aldrich. Polyimide SE 5661 was supplied by Nissan Chemical Industries. Optimizer AL 1254 was purchased from JSR. All chemicals were used as received without further purification. Their chemical structures and LC characteristics of the mixture can be seen in Fig. S1.

A.2. Preparation of LCN films

LCN films were synthesised by co-polymerisation of 24.4 wt% of diacrylate 1 and 48.8 wt% of acrylates 2 and 24.4 wt% of 3. Reactive mesogens were mixed with 1 wt% of photo absorbent dye 4, 1 wt% of photoinitiator 5 and 0.5 wt% of inhibitor 6 and dissolved in DCM to achieve homogeneous mixing. DCM was then subsequently evaporated. Glass substrates were cleaned with acetone and isopropanol in an ultrasonic bath for 20 min, dried with blown air and placed in a UV ozone for 20 min. Next, polyimides SE 5661 and AL1254 were spin-coated on the glass substrates at 5000 rpm for 40 s to induce homeotropic and planar alignment, respectively. The coated glass substrates were prebaked at 110 °C for 10 min on a hotplate and cured at 180 °C for 1.5 h in an oven. For planar alignment, AL 1254 coated glass substrates were rubbed on a velvet cloth in one direction. Glass substrates were then glued to each other with UV glue containing 20 µm spacers to fabricate cells. LC mixture was then filled into the cells at 75 °C on a hot plate. Next, the mixture in the cell was photopolymerised through a photo mask at 30 °C for 2 s with a light intensity of 30 mW/cm². In the second step, the mixture was photopolymerised at 100 °C without a photo mask for 5 min with a light intensity of 30 mW/cm². LCN film was then post-baked at 120 °C for 10 min and slowly cooled down to room temperature to release the stress induced by shrinkage due to polymerisation. Free-standing strips were removed from the cell using a razor blade and cut into desired geometries.

A.3. Simulations

The simulations were done using a Morphoshell simulation engine to predict the deformations of thin sheets based on the preferred first and second fundamental forms (30). The simulation was controlled by controlling the strain, and the second fundamental form was calculated using a formula for the curvature of a splay-bender from (29). The used meshes had 100 elements along the length and the transverse size of elements was comparable with the longitudinal one. The meshes had seams at the ends of the active segment and the clamps in order to facilitate precise control of the active ratio. The quasi-static simulations were done for increasing values of strain, if in any step the snapping was detected, the simulation step was repeated for smaller increments of strain until the desired precision was achieved.

A.4. Material characterisation

Analysis of LC phases was performed with dynamic scanning calorimetry (DSC) using a DSC Q1000 from TA instruments. LC mixture for DSC analysis was prepared without a photoinitiator. The sample was heated to 100 °C and cooled down to −50 °C at a rate of 10 °C/min in two consecutive cycles; results of the second cycle were used. A Leica CTR6000 polarised optical microscope, equipped with a Leica DFC 420C camera, was used to observe transition temperatures and alignment. Images were taken using a Leica DFC 420C camera, and the temperature was controlled using a Linkam temperature control stage. In order to measure the spontaneous curvature of the LCN strips with splay alignment, 1 × 9 mm samples with 8 mm active segments were clamped from one end (passive segment) and heated from 20 °C

to 115 °C with a rate of 5 °C/min in an oven. Temperature in the oven was tracked with a temperature and humidity sensor (SHT35-DIS-B). Curvature was calculated by image analysis. Dynamic Mechanical Analysis (DMA) was performed using Q800 DMA from TA Instruments to investigate the mechanical properties of the LCN. The sample for DMA was polymerised above the isotropic temperature in order to prevent measurement errors due to spontaneous curvature. The multi-frequency-strain mode was used, and the temperature of the strip was increased between 35 °C to 150 °C with a rate of 3 °C/min. Absorption spectra of the LCN films were obtained by UV/VIS/NIR spectrometer (Perkin Elmer Lambda 950) to investigate the absorbance of the LCN strip with dye IR 788. Absorption peaks of the photothermal dye in LCN were observed at 721 and 786 nm, with higher absorption at lower wavelengths, which can be seen in Fig. S4. Previously, these peaks were assigned to H-type aggregates of the dyes which do not affect the efficiency of heat generation [36].

A.5. Actuation

For the examination of snap-through actuation, samples were fixed at both ends and placed into the setup where they buckled to create bistable arches. Strips were placed so that planar alignment is on the bottom and homeotropic alignment is on the top of the curvature to induce snap-through deformation. Thermal actuation was performed in an oven and temperature was tracked with a digital temperature and humidity controller (SHT35-DIS-B). For photothermal actuation, an IR light of 780 nm (Thorlabs M780L3) with a collimation adapter (Thorlabs SM2F32-1) was used. Photothermal actuation of the LCN strips was achieved by illuminating the samples with a 780 nm LED light which can be absorbed by the photothermal dye incorporated into the structure of LCN and heat the network. Samples were placed 10.5 cm below the collimator adapter and irradiated with 800 mA current with a corresponding intensity of 90 mW/cm² during photothermal actuation. The light spot had an area of 2.56 cm² and FWHM of 10 mm. The surface temperature of the strips was tracked with the Xenics Gobi high-speed IR camera. For the demonstration of the throwing task, strips were covered with pearl beads of 2 µm diameter in order to prevent adhesion between the strip and the paper. Actuation videos were recorded with an Olympus digital camera. High-speed videos were recorded with a Phantom VEO1310L camera at 1000 fps. Image analysis was then performed with Blender. The centre of mass of active segments was tracked with a custom script to calculate the displacement and the peak velocity during snap-through. The images were analysed without any modification.

A.6. Power density estimation

Power density was calculated using the following formula

$$PD = \frac{m \cdot a \cdot v}{V_a}, \quad (A.1)$$

where m , a and v are the mass, acceleration and velocity of the object at the moment of peak power, and V_a is the volume of the active segment.

Appendix B. Supplementary data

Supplementary material related to this article can be found online at <https://doi.org/10.1016/j.eml.2024.102149>.

References

- [1] Y. Chi, Y. Li, Y. Zhao, Y. Hong, Y. Tang, J. Yin, Bistable and multistable actuators for soft robots: Structures, materials, and functionalities, *Adv. Mater.* 34 (19) (2022) 2110384, <http://dx.doi.org/10.1002/adma.202110384>.
- [2] Y. Forterre, J.M. Skotheim, J. Dumals, L. Mahadevan, How the Venus fly-trap snaps, *Nature* 433 (7024) (2005) 421–425, <http://dx.doi.org/10.1038/nature03185>.
- [3] H. Lee, C. Xia, N.X. Fang, First jump of microgel; Actuation speed enhancement by elastic instability, *Soft Matter* 6 (18) (2010) 4342–4345, <http://dx.doi.org/10.1039/c0sm00092b>.
- [4] Q. Zhao, X. Yang, C. Ma, D. Chen, H. Bai, T. Li, W. Yang, T. Xie, A bioinspired reversible snapping hydrogel assembly, *Mater. Horiz.* 3 (5) (2016) 422–428, <http://dx.doi.org/10.1039/c6mh00167j>.
- [5] Y. Kim, J. van den Berg, A.J. Crosby, Autonomous snapping and jumping polymer gels, *Nature Mater.* 20 (12) (2021) 1695–1701, <http://dx.doi.org/10.1038/s41563-020-00909-w>.
- [6] C.Y. Li, S.Y. Zheng, X.P. Hao, W. Hong, Q. Zheng, Z.L. Wu, Spontaneous and rapid electro-actuated snapping of constrained polyelectrolyte hydrogels, *Sci. Adv.* 8 (15) (2022) 1–11, <http://dx.doi.org/10.1126/sciadv.abm9608>.
- [7] J.A. Liu, J.H. Gillen, S.R. Mishra, B.A. Evans, J.B. Tracy, Photothermally and magnetically controlled reconfiguration of polymer composites for soft robotics, *Sci. Adv.* 5 (8) (2019) <http://dx.doi.org/10.1126/sciadv.aaw2897>.
- [8] S. Wu, G.L. Baker, J. Yin, Y. Zhu, Fast thermal actuators for soft robotics, *Soft Robot.* (2021) 1–9, <http://dx.doi.org/10.1089/soro.2021.0080>.
- [9] M. Warner, E.M. Terentjev, *Liquid Crystal Elastomers*, vol. 120, Oxford University Press, 2007, <http://dx.doi.org/10.1093/oso/9780198527671.001.0001>.
- [10] T.J. White, D.J. Broer, Programmable and adaptive mechanics with liquid crystal polymer networks and elastomers, *Nature Mater.* 14 (11) (2015) 1087–1098, <http://dx.doi.org/10.1038/nmat4433>.
- [11] G.N. Mol, K.D. Harris, C.W. Bastiaansen, D.J. Broer, Thermo-mechanical responses of liquid-crystal networks with a splayed molecular organization, *Adv. Funct. Mater.* 15 (7) (2005) 1155–1159, <http://dx.doi.org/10.1002/adfm.200400503>.
- [12] M.E. McConney, A. Martinez, V.P. Tondiglia, K.M. Lee, D. Langley, I.I. Smalyukh, T.J. White, Topography from topology: Photoinduced surface features generated in liquid crystal polymer networks, *Adv. Mater.* 25 (41) (2013) 5880–5885, <http://dx.doi.org/10.1002/adma.201301891>.
- [13] L.T. De Haan, V. Gimenez-Pinto, A. Konya, T.S. Nguyen, J.M. Verjans, C. Sánchez-Somolinos, J.V. Selinger, R.L. Selinger, D.J. Broer, A.P. Schenning, Accordion-like actuators of multiple 3D patterned liquid crystal polymer films, *Adv. Funct. Mater.* 24 (9) (2014) 1251–1258, <http://dx.doi.org/10.1002/adfm.201302568>.
- [14] T.H. Ware, M.E. McConney, J.J. Wie, V.P. Tondiglia, T.J. White, Voxellated liquid crystal elastomers, *Science* 347 (6225) (2015) 982–984, <http://dx.doi.org/10.1126/science.1261019>.
- [15] M. Barnes, R. Verduzco, Direct shape programming of liquid crystal elastomers, *Soft Matter* 15 (5) (2019) 870–879, <http://dx.doi.org/10.1039/C8SM02174K>.
- [16] K. Bhattacharya, R.D. James, The material is the machine, *Science* 307 (5706) (2005) 53–54, <http://dx.doi.org/10.1126/science.1100892>.
- [17] T. Guin, M.J. Settle, B.A. Kowalski, A.D. Augustine, R.V. Beblo, G.W. Reich, T.J. White, Layered liquid crystal elastomer actuators, *Nat. Commun.* 9 (1) (2018) 2531, <http://dx.doi.org/10.1038/s41467-018-04911-4>.
- [18] J. Hu, X. Li, Y. Ni, S. Ma, H. Yu, A programmable and biomimetic photo-actuator: a composite of a photo-liquefiable azobenzene derivative and commercial plastic film, *J. Mater. Chem. C* 6 (40) (2018) <http://dx.doi.org/10.1039/C8TC03693D>.
- [19] S. Palagi, A.G. Mark, S.Y. Reigh, K. Melde, T. Qiu, H. Zeng, C. Parmeggiani, D. Martella, A. Sanchez-Castillo, N. Kapernaum, F. Giesselmann, D.S. Wiersma, E. Lauga, P. Fischer, Structured light enables biomimetic swimming and versatile locomotion of photoresponsive soft microrobots, *Nature Mater.* 15 (6) (2016) 647–653, <http://dx.doi.org/10.1038/nmat4569>.
- [20] H. Shahsavani, A. Aghakhani, H. Zeng, Y. Guo, Z.S. Davidson, A. Priimagi, M. Sitti, Bioinspired underwater locomotion of light-driven liquid crystal gels, *Proc. Natl. Acad. Sci. USA* 117 (10) (2020) 5125–5133, <http://dx.doi.org/10.1073/pnas.1917952117>.
- [21] A.H. Gelebart, D. Jan Mulder, M. Varga, A. Konya, G. Vantomme, E.W. Meijer, R.L. Selinger, D.J. Broer, Making waves in a photoactive polymer film, *Nature* 546 (7660) (2017) 632–636, <http://dx.doi.org/10.1038/nature22987>.
- [22] X. Yang, Y. Chen, X. Zhang, P. Xue, P. Lv, Y. Yang, L. Wang, W. Feng, Bioinspired light-fueled water-walking soft robots based on liquid crystal network actuators with polymerizable miniaturized gold nanorods, *Nano Today* 43 (2022) <http://dx.doi.org/10.1016/j.nantod.2022.101419>.
- [23] J.-a. Lv, Y. Liu, J. Wei, E. Chen, L. Qin, Y. Yu, Photocontrol of fluid slugs in liquid crystal polymer microactuators, *Nature* 537 (7619) (2016) 179–184, <http://dx.doi.org/10.1038/nature19344>.
- [24] K. Dradrach, M. Zmysłony, Z. Deng, A. Priimagi, J. Biggins, P. Wasylyczyk, Light-driven peristaltic pumping by an actuating splay-bend strip, *Nature Commun.* 14 (1) (2023) 1877, <http://dx.doi.org/10.1038/s41467-023-37445-5>.
- [25] S. Timoshenko, Analysis of bi-metal thermostats, *J. Opt. Soc. Am.* 11 (3) (1925) 233–255, <http://dx.doi.org/10.1364/JOSA.11.000233>.
- [26] M. Ravi Shankar, M.L. Smith, V.P. Tondiglia, K.M. Lee, M.E. McConney, D.H. Wang, L.S. Tan, T.J. White, Contactless, photoinitiated snap-through in azobenzene-functionalized polymers, *Proc. Natl. Acad. Sci. USA* 110 (47) (2013) 18792–18797, <http://dx.doi.org/10.1073/pnas.1313195110>.
- [27] C.P. Ambulo, J.J. Burroughs, J.M. Boothby, H. Kim, M.R. Shankar, T.H. Ware, Four-dimensional Printing of Liquid Crystal Elastomers, *ACS Appl. Mater. Interfaces* 9 (42) (2017) 37332–37339, <http://dx.doi.org/10.1021/acsami.7b11851>.

- [28] J. Gao, A. Clement, M. Tabrizi, M.R. Shankar, Molecularly directed, geometrically latched, impulsive actuation powers sub-gram scale motility, *Adv. Mater. Technol.* 7 (5) (2022) 2100979, <http://dx.doi.org/10.1002/admt.202100979>.
- [29] Y. Zhao, Y. Hong, F. Qi, Y. Chi, H. Su, J. Yin, Self-Sustained Snapping Drives Autonomous Dancing and Motion in Free-Standing Wavy Rings, *Adv. Mater.* 35 (7) (2023) 1–10, <http://dx.doi.org/10.1002/adma.202207372>.
- [30] D.S. Kim, Y.J. Lee, Y.B. Kim, Y. Wang, S. Yang, Autonomous, untethered gait-like synchronization of lobed loops made from liquid crystal elastomer fibers via spontaneous snap-through, *Sci. Adv.* 9 (20) (2023) eadh5107, <http://dx.doi.org/10.1126/sciadv.adh5107>.
- [31] J. Jeon, J.C. Choi, H. Lee, W. Cho, K. Lee, J.G. Kim, J.W. Lee, K.I. Joo, M. Cho, H.R. Kim, J.J. Wie, Continuous and programmable photomechanical jumping of polymer monoliths, *Mater. Today* 49 (October) (2021) 97–106, <http://dx.doi.org/10.1016/j.mattod.2021.04.014>.
- [32] T.S. Hebner, K. Korner, C.N. Bowman, K. Bhattacharya, T.J. White, Leaping liquid crystal elastomers, *Sci. Adv.* 9 (3) (2023) 1–9, <http://dx.doi.org/10.1126/sciadv.ade1320>.
- [33] M. Warner, C.D. Modes, D. Corbett, Curvature in nematic elastica responding to light and heat, *Proc. R. Soc. Lond. Ser. A Math. Phys. Eng. Sci.* 466 (2122) (2010) 2975–2989, <http://dx.doi.org/10.1098/rspa.2010.0135>.
- [34] D. Duffy, J.S. Biggins, Defective nematogenesis: Gauss curvature in programmable shape-responsive sheets with topological defects, *Soft Matter* 16 (2020) 10935–10945, <http://dx.doi.org/10.1039/D0SM01192D>.
- [35] M. Warner, C. Modes, D. Corbett, Suppression of curvature in nematic elastica, *Proc. R. Soc. Lond. Ser. A Math. Phys. Eng. Sci.* 466 (2124) (2010) 3561–3578, <http://dx.doi.org/10.1098/rspa.2010.0139>.
- [36] M.A.M.E. Vertommen, Near-Infrared Induced Release for Localized On-Demand Drug Delivery (Ph.D. thesis), Eindhoven University of Technology, 2009, <http://dx.doi.org/10.6100/IR652929>.